ChemPubSoc Europe

DOI: 10.1002/ejic.201800090

EurJIC European Journal of Inorganic Chemistry

Full Paper

Non-Oxido Vanadium(IV) Complexes

$V^{IV}O$ and V^{IV} Species Formed in Aqueous Solution by the Tridentate Glutaroimide–Dioxime Ligand – An Instrumental and Computational Characterization

Daniele Sanna,[a] Valeria Ugone,[b] Giuseppe Sciortino,[b,c] Bernard F. Parker,[d,e] Zhicheng Zhang,[d] Christina J. Leggett,[d] John Arnold,[d,e] Linfeng Rao,*[d] and Eugenio Garribba*[b]

Abstract: Complexation of V^{IV} in aqueous solution with glutaroimide–dioxime (H_3L), a ligand proposed for the possible sequestration of uranium from seawater, was studied by the combined application of spectroscopic (EPR and UV/Vis), spectrometric (ESI-MS), electrochemical (CV), and computational (DFT) techniques. The results indicate that a rare non-oxido V^{IV} species, with formula $[V^{IV}L_2]^{2-}$, is formed in the pH range 3–5. It transforms into a usual $V^{IV}O$ complex, $[V^{IV}OL(OH)]^{2-}$, at pH > 6. The non-oxido species is characterized by a "**type 3**" EPR spectrum with $A_z \approx 126 \times 10^{-4}$ cm^{-1} and a UV/Vis signal with $\varepsilon > 2000$ M^{-1} cm^{-1} in the visible region. The detection of V^{V} species by ESI-MS spectrometry was related to two possible oxidation processes, the first one in solution and the second one in-source during the recording of the spectra. The cyclic voltammogram of $[V^{IV}L_2]^{2-}$ shows two quasi-reversible processes, at $E_{1/2} = -0.75$ V and $E_{1/2} = 0.03$ V, assigned to the V^{IV}/V^{III} reduction and V^{IV}/V^{V} oxidation, respectively. All the experimental results were verified by DFT calculations, which indicated that the geometry of the non-oxido V^{IV} complex is intermediate between an octahedron and a trigonal prism and allowed us to predict its ^{51}V hyperfine coupling (HFC) tensor ***A***, the electron absorption spectrum, the two redox processes in the cyclic voltammogram, and the electronic structure that, in turn, determines its EPR and UV/Vis behavior.

Introduction

Vanadium belongs to the ultratrace metals, which have a nutritional requirement of less than 1 mg/kg diet and are present in tissues in the range of some µg per kg. Plenty of evidence suggests that V is beneficial to human health, but the mechanism of its action remains unclear.[1] Furthermore, a number of studies have shown that vanadium compounds have therapeutic effects.[2–4] For example, recent investigations on the structure–activity[5] and reactivity–activity relationships[6] have demonstrated that V complexes exhibit a wide variety of pharmacological properties and these species have been tested in vitro or in vivo as spermicidal, anti-HIV, antiparasitic, antiviral, antitubercolotic[3,4,7] and, particularly, antidiabetic and antitumor potential agents.[4,8] The interaction of vanadium with proteins plays a fundamental role in these actions and determines the active species in the organism.[9]

Vanadium has also been found to exist in many naturally occurring compounds and plays a number of roles in biological systems.[10] For example, it is present in two enzymes, vanadium dependent haloperoxidases[11] and nitrogenases,[12] and is accumulated in the vanadocytes of ascidians and polychaete worms,[13] and in mushrooms of the genus *Amanita*.[14]

Vanadium presents a very rich chemistry and forms compounds in several oxidation states (mainly +III, +IV and +V), a variety of cations and oxidocations (V^{3+}, V^{4+}, V^{5+}, $V^{IV}O^{2+}$, $V^{V}O_2^{+}$, $V^{V}O^{3+}$), and complexes with various coordination geometries (octahedral, trigonal prismatic, square pyramidal, trigonal bipyramidal).[15] Concerning the oxidation state +IV, the compounds of the oxidovanadium(IV) ion ($V^{IV}O^{2+}$) dominate over the so-called bare or non-oxido vanadium(IV) species.[15]

An interesting fact is that the rare and unusual family of bare V^{IV} compounds are of great importance in biology, since V is accumulated in three species of mushrooms *Amanita* (*A. muscaria*, *A. regalis* and *A. Velatipes*) as a non-oxido complex named amavadin.[14,15] In *A. muscaria*, the vanadium content exceeds 400 times the value normally detected in other species of the same genus and is independent of the V concentration in the soil. The formation of amavadin, isolated in 1973 by Bayer,[16] is favored by the binding of a low molecular mass ligand, *N*-

[a] *Istituto CNR di Chimica Biomolecolare, Trav. La Crucca 3, 07040 Sassari, Italy*
[b] *Dipartimento di Chimica e Farmacia, Università di Sassari, Via Vienna 2, 07100 Sassari, Italy*
E-mail: garribba@uniss.it
https://www.dcf.uniss.it/en
[c] *Departament de Química, Universitat Autònoma de Barcelona, 08193 Cerdanyola del Vallés, Barcelona, Spain*
[d] *Chemical Sciences Division, Lawrence Berkeley National Laboratory, 1 Cyclotron Road, Berkeley, CA 94720, United States*
E-mail: lrao@lbl.gov
https://commons.lbl.gov/display/csd/
[e] *Department of Chemistry, University of California, Berkeley, CA 94720, United States*
Supporting information and ORCID(s) from the author(s) for this article are available on the WWW under https://doi.org/10.1002/ejic.201800090.

hydroxyimino-2,2′-diisopropionic acid [(*S*,*S*)-H_3hidpa], in its trianionic form hidpa(3-).[14,15] Another interesting feature of amavadin and its derivatives is their catalytic activity.[17] They have been used as catalysts for hydroxylation, oxygenation, peroxidative halogenation of alkanes and benzene,[18] peroxidative oxygenation of benzene and mesitylene,[19] and carboxylation of alkanes.[20] These facts have stimulated substantial interest in the research toward the synthesis of new bare V^{IV} compounds. As a result, structures with coordination VO_3S_3,[21] VO_6,[22] VS_6,[23] VO_4N_2,[24] VO_4X_2 (X = S, Se, P),[25] VX_2O_4 and VX_2S_4 (X = Cl, Br),[26] and $VO_2N_2S_2$[27] have been reported in the literature. The major goal of these papers was also to study the anomalous structure, electronic and spectroscopic properties of these species. Depending on the organic ligand, it is possible to obtain bare V^{IV} compounds with various types of geometry (octahedral and trigonal prismatic)[28] and isomerism (*facial* or *meridional* when the ligand is tridentate)[24c,25] with the ground state varying accordingly.[29] In the case of octahedral structures and *meridional* coordination, the ground state is based on the V-d_{xy} orbital. In contrast, a mixture of V-d_{xy}, V-d_{xz}, V-d_{yz}, V-$d_{x^2-y^2}$ and V-d_{z^2} orbitals is predicted if the ligand presents a *facial* coordination and the geometry is close to the trigonal prism. Concerning the spectroscopy behavior, in our recent EPR studies, the spectra of non-oxido V^{IV} compounds were divided into three types, "**type 1**", "**type 2**", and "**type 3**", on the basis of the largest value of the ^{51}V hyperfine coupling (HFC) tensor ***A*** and on the composition of the singly occupied molecular orbital (SOMO). The spectra of "**type 1**" are detected for V^{IV} species formed by tridentate ligands with rigid structure and *meridional* coordination (the spectrum of amavadin falls in this class), the spectra of "**type 2**" are observed for bidentate ligands which form trigonal prismatic structures and the spectra of "**type 3**" are revealed for V^{IV} species formed with tridentate ligands with a flexible structure. The electronic absorption spectra of non-oxido V^{IV} species also show peculiar features that differ from those of oxido V^{IV} species. For example, the absorption bands of oxido V^{IV} species in the visible range are mainly pure d–d transitions with low values of the molar absorption coefficient (ε), while the absorption bands for bare V^{IV} species in the range 400–800 nm are dominated by metal-to-ligand charge transfer (MLCT) and ligand-to-metal charge transfer (LMCT) transitions, with very high values of ε (from 1000 to 50000 M^{-1} cm^{-1}).

Very recently, some of us demonstrated that glutaroimide–dioxime (H_3L) (shown in Scheme 1) forms a very stable bare V^V complex with composition $[V^VL_2]^-$ in aqueous solution, isolable also in the solid state,[30] which has important implications in the interference of vanadium during the recovery of uranium from seawater through specific ligands such as poly(amidoximes). The logical consequence is to try to synthesize a possible bare vanadium species from solutions containing V^{IV}. Therefore, in this work we studied the behavior of the system V^{IV}/glutaroimide–dioxime (H_3L) in aqueous solution and characterized a new non-oxido V^{IV} species through a combination of spectroscopic, spectrometric, electrochemical, and computational methods. The electronic structure of this complex was also discussed and compared with that of other similar compounds. The new V^{IV} species formed with glutaroimide–dioxime (H_3L) enriches the list of this type of complexes and adds new insights in the comprehension of the structure and characterization of the properties of bare vanadium(IV) compounds.

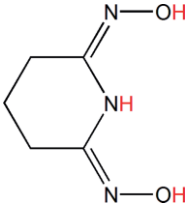

Scheme 1. Structure of glutaroimide–dioxime (H_3L). The three dissociable protons in the presence of V^{IV} and V^V are indicated in red.

Results and Discussion

The Ligand

The glutaroimide–dioxime ligand in the fully protonated form can be indicated with H_4L^+ with two protons on the imide group $-NH_2^+$ and two on the oxime groups. Only three deprotonations can be observed for the free ligand and they have been reported recently in the literature. They were attributed to the imide group (pK_{a1} = 2.12) and to the stepwise deprotonations of the oxime groups –NOH (pK_{a2} = 10.70 and pK_{a3} = 12.06).[31] The values for pK_{a2} and pK_{a3} indicate that the deprotonation of these groups is not completely independent.[31a] The deprotonation of the imide group –NH in the neutral form cannot be measured in water and is induced by complexation with metal ions.[30,31]

In this study, the three pK_a values were confirmed by DFT methods following the procedure described by Liptak et al.[32] The details of the calculations are given in the Supporting Information. An explicit cluster of water molecules was adopted to take into account the solvent stabilization of the acidic groups (9 water molecules solvating the oxime groups and 2 the imide group, Figures S1 and S2). The results listed in Table S1 (pK_{a1} = –9.2, pK_{a2} = 13.4, and pK_{a3} = 17.4) were coherent with the values in the literature,[31] suggesting a favorable deprotonation of the positively charged imide group and a high value of pK_a for the two oxime groups. The difference between pK_{a2} and pK_{a3} confirms that these deprotonation steps are not independent, in agreement with the experimental data.

Studies in Aqueous Solution

Anisotropic EPR spectra were recorded as a function of pH in the system containing $V^{IV}O^{2+}$ ion and H_3L at metal to ligand molar ratio of 1:3. At pH = 2.4, only the $[V^{IV}O(H_2O)_5]^{2+}$ aquaion exists in aqueous solution (resonances indicated with **I** in Figure 1). When the pH is raised to about 3, new signals appear and indicate the formation of new species (resonances **II** in Figure 1). The small value of ^{51}V hyperfine coupling constant *A* (126.4×10^{-4} cm^{-1}) for this species would suggest it is a non-oxido V^{IV} complexes, structurally analogous to the compound revealed in the system containing V^V.[30] If the ligand is indi-

cated with H_3L, to this complex the formula $[V^{IV}L_2]^{2-}$, with $2 \times (O^-, N^-, O^-)$ coordination, could be assigned. It can be noticed that, in the pH range 3.0–5.0, no other V^{IV} species are present in solution. This complex survives until pH 5.5, even if the signal intensity decreases with increasing pH. This fact could indicate hydrolysis and/or oxidation processes, which should give $[V^{IV}O(OH)]^+$ and $[(V^{IV}O)_2(OH)_2]^{2+}$,[33] and/or EPR-silent V^V species. At pH > 5.0, another complex appears in solution (resonances indicated with **III** in Figure 1). The value of A_z for this species (142.4×10^{-4} cm^{-1}) is significantly higher than that of non-oxido complex (126.4×10^{-4} cm^{-1}), which would indicate that a $V^{IV}O$ species is formed upon the hydrolysis of $[V^{IV}L_2]^{2-}$ to give $[V^{IV}OL(OH)]^{2-}$ according to reaction (1).

$$[V^{IV}L_2]^{2-} + 2\ H_2O \rightleftarrows [V^{IV}OL(OH)]^{2-} + H_3L \quad (1)$$

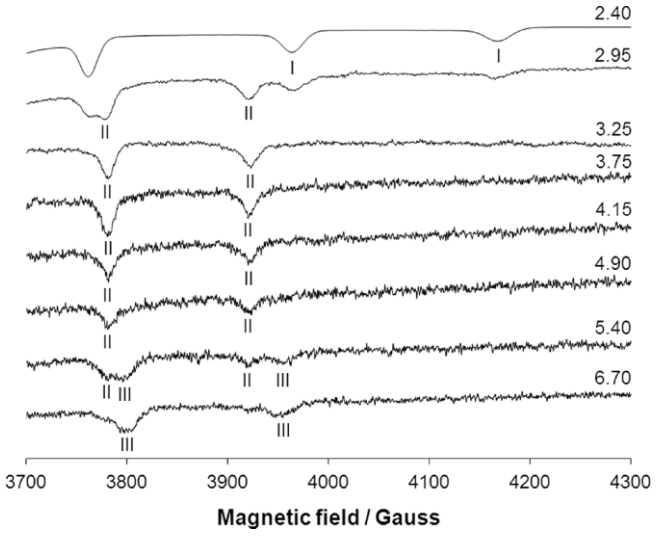

Figure 1. High field region of the X-band anisotropic EPR spectra recorded as a function of pH in the system $V^{IV}O^{2+}/H_3L$ with V^{IV} concentration of 1.0×10^{-3} M and metal to ligand molar ratio of 1:3. The M_I = 5/2, 7/2 resonances of $[V^{IV}O(H_2O)_5]^{2+}$, $[V^{IV}L_2]^{2-}$ and $[V^{IV}OL(OH)]^{2-}$, are denoted as **I**, **II**, and **III**, respectively.

The value of A_z for $[V^{IV}OL(OH)]^{2-}$ is compatible with an [(O^-, N^-, O^-); OH^-] equatorial coordination, for which the "additivity relationship"[34] predicts a value around $145–146 \times 10^{-4}$ cm^{-1}. As a verification, we also performed DFT calculations to optimize the structure of $[V^{IV}OL(OH)]^{2-}$ (Figure S3 of the Supporting Information) and calculated the value of A_z with ORCA software at the level of theory PBE0/VTZ, which allows to obtain predictions with a percent deviation (PD) smaller than 3 % from the experimental value for $V^{IV}O$ with (N,O) ligands.[35] The calculated value, $|A_z|^{calcd}$, is 144.1×10^{-4} cm^{-1} with a PD of 1.2 % from $|A_z|^{exptl}$.

At basic pH, the EPR signal disappears completely.

ESI-MS experiments using $V^{IV}OSO_4$ as the initial material were conducted to confirm the results of EPR spectroscopy. The spectra were recorded in positive and negative modes with a V final concentration of 5.0×10^{-6} M and pH in the range 4.3–6.7. The mass spectrum recorded in the negative mode at pH 4.3 (Figure 2) is characterized by three major peaks, attributed to the ligand in the monoanionic form $[H_2L]^-$ (m/z = 142.06), and to two V^V species, $[V^VO(OH)L]^-$ or $[V^VO_2L+H]^-$ (m/z = 223.99) and $[V^VL_2]^-$ (m/z = 331.04). The comparison between the experimental and calculated isotopic pattern of the peaks due to $[H_2L]^-$, $[V^VO(OH)L]^-$/$[V^VO_2L+H]^-$ and $[V^VL_2]^-$ ions is reported in Figures S4–S6 of the Supporting Information, in which the satellite peaks, due to the natural abundance of ^{13}C isotope, are separated by $m/z \approx 1.00$ for these fragments with charge of –1 and allowed us to confirm the attribution proposed. The two V^V complexes were observed in a recent paper, and their existence in aqueous solution was related to the use of NaV^VO_3 as the metal salt.[30] In contrast, using $V^{IV}OSO_4$, one would expect signals ascribable to V^{IV} adducts, which – instead – were not detected even if the latter were well visible in the EPR spectra in Figure 1.

The detection of V^V species can be related to two concomitant oxidation processes, the first one in solution and the second one in-source during the recording of the spectra.[36,37] The presence of an OH^- ion in the equatorial plane of $[V^{IV}OL(OH)]^{2-}$ should favor the oxidation to $[V^VO(OH)L]^-$/$[V^VO_2L+H]^-$, according to the mechanism suggested in Scheme 2.

The ESI mass spectra recorded in the positive mode were not informative, indicating that the V species formed in solution are negatively charged.

To shed light on the oxidation process observed with ESI-MS spectrometry, the intensity of the EPR signals of $[V^{IV}L_2]^{2-}$ species was monitored as a function of time and reported in Figure 3. The experimental points refer to the intensities of the resonances M_I = –7/2 and –5/2 along the z axis. As it can be observed, the oxidation is not very fast. The EPR intensity is reduced to 50 % after more than 30 min and the spectral signal

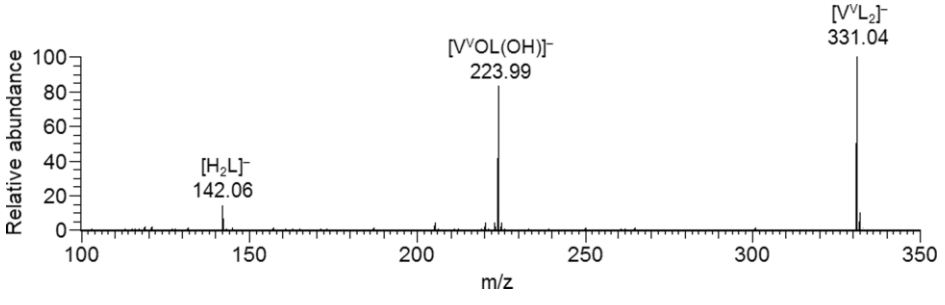

Figure 2. ESI mass spectrum recorded in the negative mode at pH 4.30 in ultrapure water in the system $V^{IV}O^{2+}/H_3L$ with a molar ratio of 1:3 and V concentration of 5.0×10^{-6} M.

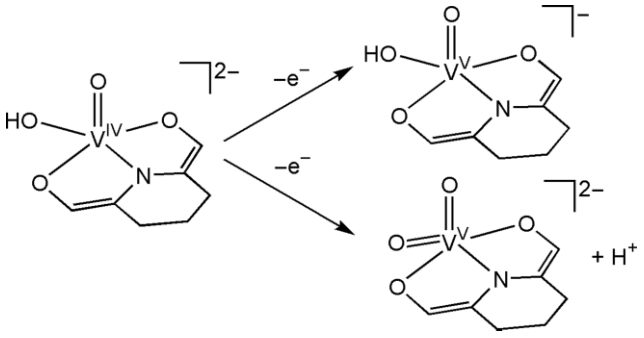

Scheme 2. Possible oxidation mechanisms of $[V^{IV}OL(OH)]^{2-}$ to $[V^{V}O(OH)L]^{-}$ (above) or $[V^{V}O_2L]^{2-}$ (below).

is still 30 % of the initial value after two hours. This would suggest that only a portion of V^{IV} undergoes oxidation in aqueous solution, while the remaining part is oxidized in-source during the recording of the ESI-MS spectra, in agreement with what was discussed in the literature.[36]

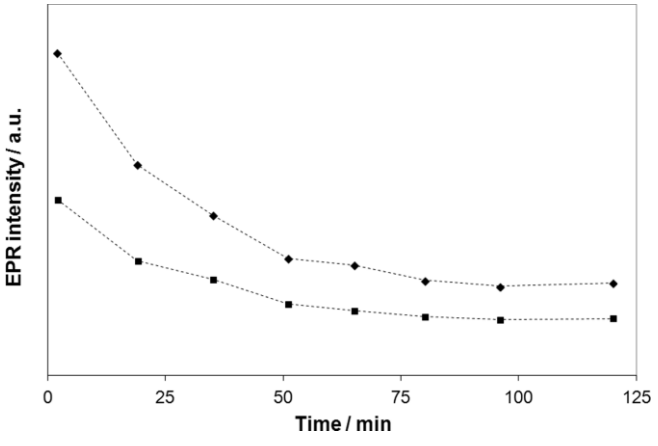

Figure 3. Intensity of the EPR signals of $[V^{IV}L_2]^{2-}$ measured as a function of time (V^{IV} 1.0×10^{-3} M, metal to ligand molar ratio 1:3, pH 3.55). Rhombi (above) and squares (below), indicate the intensity of the M_I = –5/2 and –7/2 resonances (along the *z* axis), respectively.

Characterization of the Non-Oxido V^{IV} Complex

Optimization of the Structure

A hexacoordinate structure formed by a tridentate ligand can be described in terms of its isomerism, *meridional* (*mer*) or *facial* (*fac*). A high rigidity of the ligand favors the *meridional* coordination, as observed for the metal complexes of 3,5-bis(2-hydroxyphenyl)-1-phenyl-1*H*-1,2,4-triazole (H_2hyph^{Ph}) and 2,6-bis(2-hydroxyphenyl)pyridine (H_2bhpp).[38–40] For tridentate ligands with a flexible backbone, such as iminodiacetic acid, an intermediate structure between the *meridional* and *facial* is usually observed.[41] The two situations for a (O,N,O) ligand are shown in Scheme 3. An intermediate geometry is also expected for glutaroimide–dioxime (H_3L).

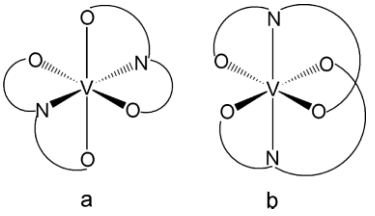

Scheme 3. Possible hexacoordinate structures for a non-oxido vanadium(IV) complex formed by a tridentate (O,N,O) ligand: (a) *fac* and (b) *mer*.

The geometry of $[V^{IV}L_2]^{2-}$ species was calculated with Gaussian 09 software through DFT methods, using the functional B3P86 and the valence triple-ζ basis set 6-311g, according to the procedure established in the literature for vanadium complexes.[42] The optimized structure is shown in Figure 4. In Table 1 the geometrical parameters calculated for $[V^{IV}L_2]^{2-}$ and the experimental and calculated structural details for the analogous species of V^{V}, $[V^{V}L_2]^{-}$, are given. Overall, it can be noticed that there is good agreement between the experimental and optimized V^{V} structure, even if large deviations are observed for the N–V–N bond angle. As expected, V–O and V–N bonds would be longer for the V^{IV} than for the V^{V} species. The use of polarization and diffuse functions results in a slight improvement of the prediction for $[V^{V}L_2]^{-}$ [in Figure S7 of the Supporting Information the structures calculated at the level of theory B3P86/6-311g and B3P86/6-311++g(d,p) are compared with the X-ray data], while for $[V^{IV}L_2]^{2-}$ the two geometries optimized with the two basis sets are almost coincident (Figure S8).

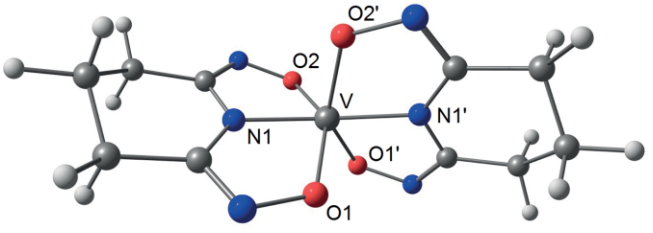

Figure 4. Structure of $[V^{IV}L_2]^{2-}$, optimized with DFT methods at the level of theory B3P86/6-311g.

Usually, a non-oxido V species can be described by several geometrical parameters:[38] (1) the "twist" angle Φ, which measures the angle between the two triangular faces of side *s* describing the coordination polyhedron (60° for an octahedron and 0° for a trigonal prism); (2) the angle Θ formed by the donors in *trans* to the vanadium (180° for an octahedron and 135° for trigonal prism); (3) the angle Ω formed by the two external donors of each ligand molecule with respect to vanadium (180° for *mer* and 90° for *fac* isomers); (4) the ratio *s*/*a* and *s*/*h*, where *a* is the mean metal–ligand bond length and *h* is the distance between the two triangular faces (they are 1.414 and 1.225 for an octahedron, and 1.309 and 1.000 for a trigonal prism). The values for the angles Φ, Θ and Ω predicted for $[V^{IV}L_2]^{2-}$ fall between those expected for a regular octahedron and a trigonal prism (24.9, 149.6 and 144.5°, respectively). Also, the ratios *s*/*h* and *s*/*a* indicate a distorted structure, intermediate between the limits represented by the octahedral and trigonal prismatic arrangements.

Table 1. Experimental and calculated geometrical parameters for non-oxido V^V and V^{IV} complexes.[a]

Parameter [b]	$[V^VL_2]^-$ (experimental) [c]	$[V^VL_2]^-$ (calculated) [d]	$[V^{IV}L_2]^{2-}$ (calculated) [d]
V–O1, V–O1′	1.867, 1.874	1.873, 1.877	1.950, 1.950
V–N1, V–N1′	1.955, 1.956	1.967, 1.967	1.982, 1.983
V–O2, V–O2′	1.902, 1.904	1.873, 1.877	1.973, 1.973
O1–V–O1′	92.2	94.0	103.7
N1–V–N1′	154.9	179.0	159.8
O2–V–O2′	97.2	94.1	86.3
Φ [e]	26.7	42.9	24.9
Θ [f]	149.6	159.1	149.6
Ω [g]	146.9	149.2	144.5
s/*a* [h]	1.360	1.424	1.378
s/*h* [i]	1.099	1.252	1.137

[a] Distance in Å and angles in degrees. [b] The numbering of the atoms is the same as used in Figure 4. [c] Experimental X-ray structure taken from ref.[30] [d] Structure simulated through DFT methods at the level of theory B3P86/6-311g. [e] Mean twist angle: 60° for octahedral and 0° for trigonal prismatic geometry. [f] Angle formed by the donors in *trans* position with vanadium (mean value): 180° for octahedral and 135° for trigonal prismatic geometry. [g] Angle formed by the two external donor atoms of the ligand with vanadium (mean value): 180° for *mer* and 90° for *fac* isomers. [h] *s* is the side of the two triangular faces which describe the coordination polyhedron and *a* is the mean metal–ligand bond length: the ratio *s*/*a* is 1.414 for an octahedron and 1.309 for a trigonal prism. [i] *s* is the side of the two triangular faces which describe the coordination polyhedron and *h* is the distance between the two faces: the ratio *s*/*h* is 1.225 for an octahedron and 1.000 for a trigonal prism.

Table 2. Experimental spin Hamiltonian parameters (*g* and *A* values) for $[V^{IV}L_2]^{2-}$ complex.[a]

Parameter	g_{iso}	g_{iso}^{expct} [b]	g_x	g_y	g_z	A_{iso}	A_{iso}^{expct} [c]	A_x	A_y	A_z
	1.973	1.973	1.988	1.977	1.955	–67.6	–68.5	–12.0	–67.0	–126.4

[a] Values of *A* reported in 10^{-4} cm^{-1} units. [b] g_{iso}^{expct} is the value of g_{iso} expected on the basis of the formula $g_{iso} = (1/3)(g_x + g_y + g_z)$. [c] A_{iso}^{expct} is the value of A_{iso} expected on the basis of the formula $A_{iso} = (1/3)(A_x + A_y + A_z)$.

Prediction of the ^{51}V Hyperfine Coupling Constants

The most frequently used technique for the characterization of V^{IV} complexes is EPR spectroscopy.[29,34a,34b] The spin Hamiltonian parameters (*g* and *A*) for $[V^{IV}L_2]^{2-}$ were determined generating the experimental spectrum with WinEPR software[43] and are reported in Table 2. The comparison between the experimental and generated spectrum is shown in Figure 5.

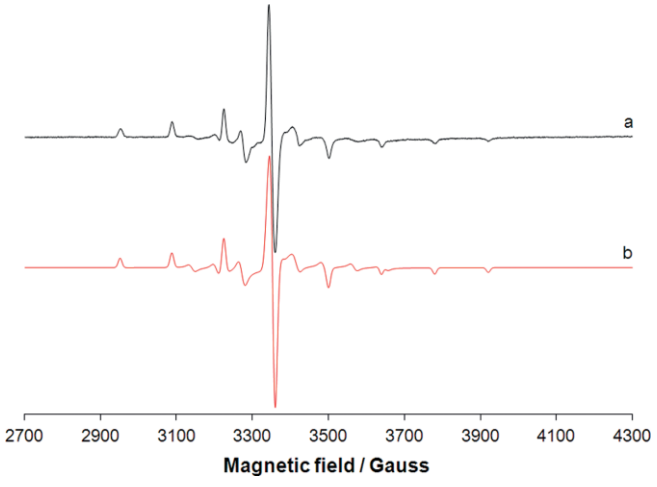

Figure 5. X-band anisotropic EPR spectrum of $[V^{IV}L_2]^{2-}$: (a) experimental and (b) generated by WinEPR software.

We recently demonstrated that the EPR spectra of hexacoordinate V^{IV} complexes can be divided into three groups: "**type 1**" spectra of species with geometry close to the octahedron and $A_z >> A_x \approx A_y$ (A_z in the range 135–155 × 10^{-4} cm^{-1}); "**type 2**" spectra due to the complexes with geometry close to the trigonal prism and $A_x \approx A_y >> A_z$ ($A_x \approx A_y$ in the range 90–120 × 10^{-4} cm^{-1}); spectra of "**type 3**" for species with geometry intermediate between the octahedron and the trigonal prism and $A_z > A_y > A_x$ or $A_x > A_y > A_z$ (A_z or A_x in the range 120–135 × 10^{-4} cm^{-1}).[44] The ground state is based on V-d_{xy} orbital for "**type 1**" spectra (percentage of V-d_{xy} in the singly occupied molecular orbital or SOMO > 90 %), while the contribution of other V-d orbitals increases in the "**type 3**" spectra (percentage of V-d_{xy} in the SOMO ≈ 60–80 %) and, above all, in the "**type 2**" spectra (percentage of V-d_{xy} in the SOMO < 40 %). For a tridentate ligand, *meridional* coordination results in a "**type 1**" spectrum, whereas *facial* coordination in a "**type 3**" spectrum.[45] On the basis of the structural data in Table 1, for $[V^{IV}L_2]^{2-}$ an intermediate spectrum of "**type 3**" is expected and the parameters listed in Table 2 confirm this insight.

Nowadays, the prediction of ^{51}V HFC tensor ***A*** is possible through the DFT methods. We recently observed that the ORCA software gives better results than popular Gaussian for non-oxido vanadium(IV) complexes, because it includes the second-order spin–orbit effects, whose contribution to *A* is more important than for $V^{IV}O$ species.[38,45,46] Among the functionals, it has been recently demonstrated that, for a bare V^{IV} complex, the double hybrid B2PLYP[47] gives a mean percentage deviation (MPD) from A_{iso} of –0.3 % if using the basis set VTZ, and from A_i ($i = x$ or z, depending on the symmetry and electronic structure of the complex) of –0.9 % if using the 6-311g(d,p) basis set.[44] The results of the DFT simulations for $[V^{IV}L_2]^{2-}$ are listed in Table 3.

In Table 3, it can be noticed that DFT calculations correctly predict the order $A_z > A_y > A_x$. The percent deviation from the experimental A_{iso} and A_z is very satisfactory, below 1 % for both

Table 3. Calculated (calcd.) and experimental (exptl.) ^{51}V hyperfine coupling constants (A) for $[V^{IV}L_2]^{2-}$ complex.[a]

A	A_{iso} [b]	A_x[c]	A_y[c]	A_z[c]	PD (A_{iso})[d]	PD (A_z)[d]
Calcd.	−66.7	−8.1	−55.4	−126.8	−1.0	0.3
Exptl.	−67.6	−12.0	−67.0	−126.4	–	–

[a] Values of A reported in 10^{-4} cm^{-1} units. [b] Functional B2PLYP and basis set VTZ. [c] Functional B2PLYP and basis set 6-311g(d,p). [d] Percent deviation from the experimental value calculated as $100 \times [(|A_i|^{calcd} - |A_i|^{exptl})/|A_i|^{exptl}]$, with i = iso or z.

the values and in line with the results recently reported.[44] The agreement is comparable with that obtained for $V^{IV}O$ complexes, for which deviations below 3 % are predicted.[35,48]

The arrangement of the ligand molecules, *mer* or *fac*, has remarkable effects on the electronic structure of a non-oxido V^{IV} complex.[27,38,45,49] In particular, the values of A can be correlated with Ω, i.e. the angle formed by the two external donors of the tridentate ligand, which is 180° for a *mer* and 90° for a *fac* isomer (see Table 1). The values of A_i (i = x, z) as a function of Ω for some tridentate ligands are shown in Figure 6. Three types of ligands were considered: (1) cyclic ligands which form *fac* structures, such as 1,3,5-triamino-1,3,5-trideoxy-*cis*-inositol,[50] 1,3,5-trideoxy-1,3,5-tris(dimethylamino)-*cis*-inositol,[50] and *cis*-inositol;[51] (2) open-chain flexible ligands which yield intermediate structures, such as 2,2′-dihydroxyazobenzene,[45] α-(2-hydroxy-5-methylphenylimino)-*o*-cresol,[45] calmagite,[45] anthracene chrome red A,[45] three dithiocarbazate-based Schiff-bases,[27] and four tridentate aroylazine ligands;[49] (3) open-chain rigid ligands which give *mer* structures, such as 3,5-bis(2-hydroxyphenyl)-1-phenyl-1*H*-1,2,4-triazole,[38] 2,6-bis(2-hydroxyphenyl)pyridine,[38] and bis(3,5-dimethyl-2-hydroxyphenyl)trimethylamine.[24c] From the examination of Figure 6, it can be noticed that A_z for $[V^{IV}L_2]^{2-}$ (pink square) falls in the region predicted for the open-chain ligands. In particular, the values of Ω of 144.5° and $|A|$ of 126.4×10^{-4} cm^{-1} correspond to a "**type 3**" EPR spectrum and are attributable to a bare V complex with geometry intermediate between the octahedron and the trigonal prism.[44]

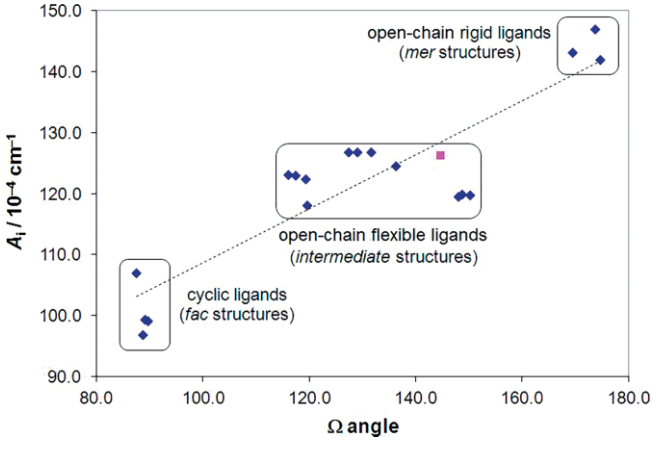

Figure 6. A_i values for non-oxido V^{IV} complexes as a function of the angle Ω. The pink square indicates $[V^{IV}L_2]^{2-}$. A_i (i = x or z) is the largest values of the ^{51}V HFC tensor ***A***. The dotted line represents the best linear fitting of the nineteen points.

Prediction of the Electronic Structure of the V^{IV} Species

For a distorted octahedral $V^{IV}O$ complex, such as $[VO(H_2O)_5]^{2+}$, the energy order of the five V-d orbitals is $d_{xy} < d_{xz} \approx d_{yz} < d_{x^2-y^2} < d_{z^2}$,[52] the singly occupied molecular orbital (SOMO, which coincides with the HOMO) being the d_{xy} orbital. For a non-oxido V^{IV} species with a hexacoordinate geometry distorted toward the trigonal prism, a significant mixing of V-d_{xy} with the unoccupied orbitals, such as V-d_{xz}, V-d_{yz}, V-$d_{x^2-y^2}$ and V-d_{z^2}, is expected.[44,53] Such a mixing causes a lowering of the absolute value (experimentally measured) of the ^{51}V hyperfine coupling constant along the x or z axis.

The analysis of the electronic structure and molecular orbital composition of $[V^{IV}L_2]^{2-}$ has been carried out by choosing a coordinate system in which the N–V–N direction is oriented along the z axis, and two O–V–O directions occupy the x and y axes. The energy levels of the molecular orbitals (MOs) derived from V-d orbitals are shown in Figure 7. For clarity, the energy of the MOs is relative to the SOMO, set as reference at 0.0 eV. The percentages shown in Figure 7 (in parenthesis) refer to the total contribution of V atomic orbitals in the specific MO, the sum of the values giving 100 %. With this approach it is easily observable the entity of the mixing of the V-d orbitals in the MOs. The five MOs with V-d character are represented in Figure 8: SOMO or HOMO with major contribution from V-d_{xy}; LUMO+2 and LUMO+3 with similar energy and mixing of V-d_{yz} and V-d_{xz}; LUMO+11 and LUMO+12 with energy comparable and contribution almost exclusively from V-$d_{x^2-y^2}$ and V-d_{z^2}, respectively. Therefore, the energy order of the MOs with V-d contribution is: $d_{xy} < d_{yz} \approx d_{xz} < d_{x^2-y^2} \approx d_{z^2}$, similar to that calculated for other bare V^{IV} species which give "**type 3**" EPR spectra.[44] It can be observed that, whereas V-$d_{x^2-y^2}$ and V-d_{z^2} scarcely combine with other V-d orbitals, a strong mixing between V-d_{xy}, V-d_{xz} and V-d_{yz} exists. Therefore, the SOMO, LUMO+2 and LUMO+3 are significantly mixed. Concerning the SOMO, the percent composition is: V-d_{xy} (81.7 %), V-d_{yz} (7.3 %), V-$d_{x^2-y^2}$ (5.6 %), V-d_{xz} (4.2 %) and V-d_{z^2} (1.1 %), in agreement with the prediction for a complex with a "**type 3**" spectrum.[44] The high contribution of V-d orbitals (55.6 % in the SOMO,

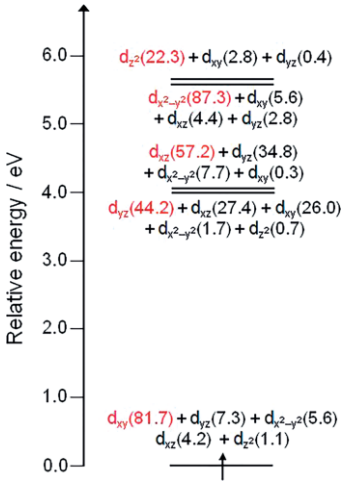

Figure 7. Relative energy levels for V-d orbitals of $[V^{IV}L_2]^{2-}$. The atomic orbital that mostly contributes to the specific MO is shown in red.

57.7 % in the LUMO+2 and 63.8 % in the LUMO+3) to the frontier MOs and the EPR results are also consistent with the observed redox activity (see below), where the processes are largely metal-based, although assisted by the ligands.

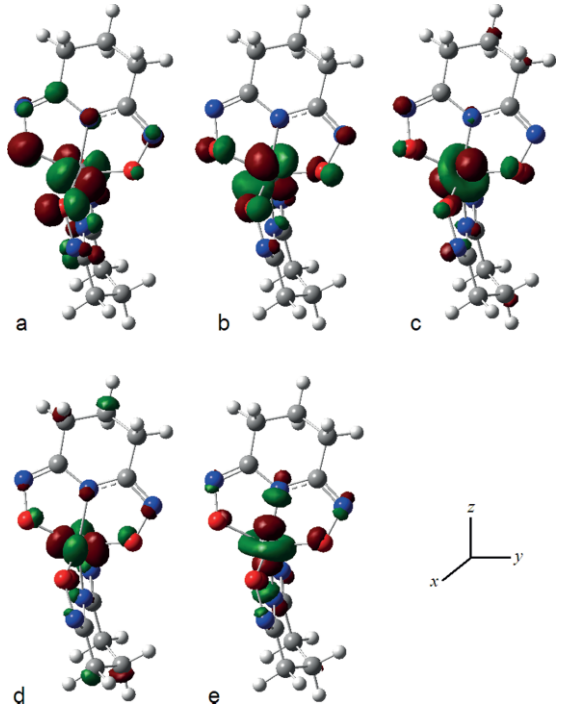

Figure 8. Molecular orbitals for $[V^{IV}L_2]^{2-}$: (a) SOMO (mixing of V-d_{xy}, V-d_{yz}, V-$d_{x^2-y^2}$ and V-d_{xz}); (b) LUMO+2 (mixing of V-d_{yz}, V-d_{xz} and V-d_{xy}); (c) LUMO+3 (mixing of V-d_{xz}, V-d_{yz} and V-$d_{x^2-y^2}$); (d) LUMO+11 (V-$d_{x^2-y^2}$); (e) LUMO+12 (V-d_{z^2}).

Prediction of the UV/Vis Spectrum

The electronic absorption spectrum of $[V^{IV}L_2]^{2-}$ was simulated by TD-DFT methods according to the procedures reported in the literature.[54] It has been recently observed that, for a bare V^{IV} complex, long-range corrected functionals, such as CAM-B3LYP, and half-and-half hybrid, such as BHandHLYP, allow predicting the UV/Vis spectra better than simple hybrid and standalone functionals.[27] Even if a quantitative agreement with the experimental spectra is not possible yet, these types of calculations satisfactorily reproduce the spectrum, both in the visible and UV regions. In this latter region, CAM-B3LYP performs better than the other functionals.

The comparison between the experimental and calculated spectrum for $[V^{IV}L_2]^{2-}$ [with CAM-B3LYP as the functional and 6-31+g(d) as the basis set] is given in Figure 9. Differing from the d–d bands of $V^{IV}O$-species, for which those observed in the visible range are almost pure d–d transitions with very low oscillator strength *f* (corresponding to molar absorption coefficient ε lower than 200 M^{-1} cm^{-1}), the d–d bands of $[V^{IV}L_2]^{2-}$ are predicted with low intensity in the near IR region (1195–1245 nm), whereas in the visible region (between 400 and 800 nm) the absorptions are mainly metal-to-ligand charge

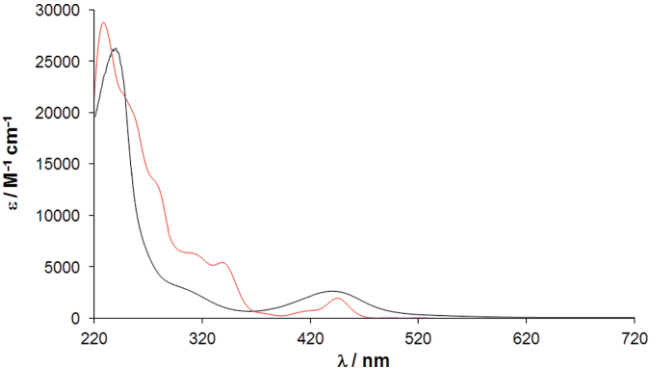

Figure 9. Experimental (in black) and calculated (in red) electronic absorption spectrum of $[V^{IV}L_2]^{2-}$. The functional and basis set used were CAM-B3LYP and 6-31+g(d), respectively.

Table 4. Calculated and experimental electronic transitions for $[V^{IV}L_2]^{2-}$ up to 220 nm.[a]

Main transition [b]	Character [c]	λ^{calcd} [d]	$f^{calcd} \times 5 \times 10^5$ [e]	$\lambda^{exptl}/\varepsilon^{exptl}$ [d,f,g]
H(α) → L+11(α)	d–d (V-d_{xy} → V-$d_{x^2-y^2}$)	1242.3	50	
H(α) → L+12(α)	d–d (V-d_{xy} → V-d_{z^2})	1197.0	300	
H-1(α) → L(α)/ H(α) → L+1(α)	LLCT/MLCT (V-d_{xy} → L)	445.2	5650	442/2670
H-2(α) → L+12(α)	LMCT (L → V-d_{z^2})	422.3	1700	419/2130 (sh)
H-1(α) → L+11(α)	LMCT (L → V-$d_{x^2-y^2}$)	410.8	850	404/1600 (sh)
H(α) → L+5(α)	MLCT (V-d_{xy} → L)	342.8	6600	332/1470 (sh)
H-1(β) → L+5(β)/ H(β) → L+6(β)	LLCT/LLCT	317.4	7800	
H-3(α) → L+11(α)/ H(β) → L+7(β)	LMCT (L → V-$d_{x^2-y^2}$)/LLCT	305.8	5700	309/2730 (sh)
H-2(β) → L+2(β)	LLCT	277.9	10450	
H-4(α) → L+13(α)	LLCT	271.9	12200	271/6330 (sh)
H-2(β) → L+6(β)/ H-2(β) → L+12(β)	LLCT/LLCT	255.4	25450	240/26270
H-1(α) → L+13(α)	LLCT	229.5	27750	

[a] Calculations performed at the level of theory CAM-B3LYP/6-31+g(d). [b] H stands for HOMO and L for LUMO, and HOMO coincides with SOMO. [c] Even if MOs are formed by the combination of various atomic orbitals, we attributed them to V or the ligands on the basis of the largest contribution in the specific MO. [d] Values of λ measured in nm. [e] Oscillator strength. [f] Values of ε measured in M^{-1} cm^{-1}. [g] The letters "sh" indicate a shoulder of a more intense absorption.

transfer (MLCT) and ligand-to-metal charge transfer (LMCT) transitions, and the MOs involved are those centered on the ligands with π character and those based on V-d orbitals such as V-d_{xy}, V-$d_{x^2-y^2}$ and V-d_{z^2}. This confirms what was discussed in the literature, i.e. that for non-oxido vanadium(IV) species most of the transitions derive from LMCT absorptions (see Table 4).[55] The oscillator strength for the excitations in the visible range is about two to three orders of magnitude larger than that of the $V^{IV}O$ complexes (ε = 2670 M^{-1} cm^{-1} for the band at 442 nm). In the UV region, the first absorptions are MLCT or LMCT, more or less until 300 nm, when the intraligand charge transfer or ligand-to-ligand charge transfer (LLCT) gains the upper hand with a significant increase of the oscillator strength which reflects the increase of the ε value (ε is 3070 M^{-1} cm^{-1} at 300 nm, whereas it rears up at 26270 M^{-1} cm^{-1} at 240 nm).

In Table 4 the most important calculated electronic transitions, expressed by absorption wavelength and oscillator strength, are compared with the experimental data.

Electrochemistry

Cyclic voltammograms of $[V^{IV}L_2]^{2-}$ have been recorded at a platinum working electrode under an atmosphere of purified argon in water (0.1 M KNO_3) at 25 °C in the potential range from –1.0 V to 1.0 V vs. Ag/AgCl reference. We used as a starting point the open circuit potential (OPC).

In the cathodic potential range an electrochemical response is observed (Figure 10). It corresponds to the half-reduction with $E_{1/2}$ = –0.75 V and can be assigned to the process $[V^{IV}L_2]^{2-} + e^- \rightleftarrows [V^{III}L_2]^{3-}$. On the basis of comparison with the $[Fe^{III}(CN)_6]^{3-}/[Fe^{II}(CN)_6]^{4-}$ couple (ΔE_p = 90 mV at a scan rate of 100 mV s^{-1}), this electrochemical response may be appropriately described as quasi-reversible (ΔE_p = 143 mV). The quasi-reversibility of one-electron oxidation and reduction has been already observed in the literature for other non-oxido V^{IV} complexes and can be explained postulating that the distorted octahedral structure around the bare vanadium ion is maintained during the reduction process.[56,57] In contrast, the reduction would be irreversible in the case of a $V^{IV}O$ complex because the process would entail the loss of the oxido ligand.[56]

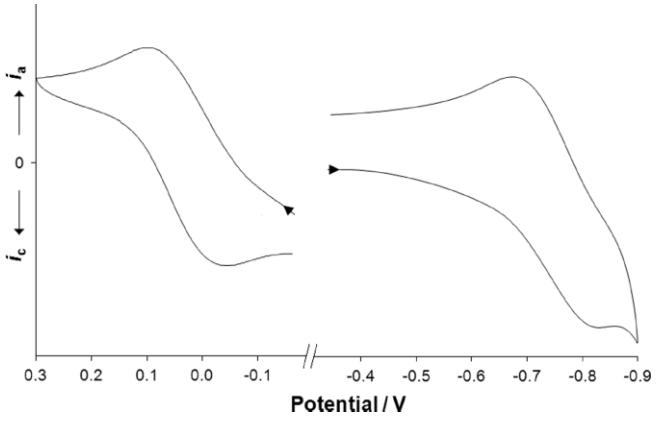

Figure 10. Cyclic voltammogram in aqueous solution at 25 °C of the anodic (left) and cathodic (right) potential range for $[V^{IV}L_2]^{2-}$ (V concentration of 1.0×10^{-3} M). Pt was used as the working electrode and the potential E was measured vs. Ag/AgCl reference (0.1 M KNO_3; scan rate 100 mV s^{-1}). The cathodic (negative) and anodic (positive) current are indicated by i_c and i_a, respectively.

When the cyclic voltammogram is recorded in the anodic range, an oxidation process is observed with $E_{1/2}$ = 0.03 V and ΔE_p = 127 mV. In this case too, the oxidation can be considered quasi-reversible because there is no structural change from distorted octahedral $[V^{IV}L_2]^{2-}$ species to $[V^{V}L_2]^{-}$.

Overall, these data are in agreement with those of other hexacoordinate bare V^{IV} species formed by tridentate ligands with (O,O,O) or (O,N,O) donors.[58] For example, the two complexes formed by 1,3,5-triamino-1,3,5-trideoxy-*cis*-inositol (taci), $[V^{IV}(taci)_2]^{4+}$, and *cis*-inositol (ino), $[V^{IV}(inoH_{-3})_2]^{2-}$, give reversible or quasi-reversible reduction (and oxidation) to the corresponding V^{III} (and V^{V}) species.[50,51] For bare V^{IV} species formed by *S*-methyl-β-*N*-(2-hydroxy-5-methylphenyl)methylenedithiocarbazate the values of ΔE_p for the quasi-reversible reduction and oxidation are 120 and 130 mV,[27] in line with those determined in this study. This behavior is explainable only if the coordination geometry and the metal environment remain the same as in the V^{IV} complex upon the redox processes.

To confirm the attribution of $E_{1/2}$ to the reduction and oxidation half-reactions, DFT calculations were carried out. In the literature it is reported that a good prediction of the reduction potential is possible with density functional theory methods, even if a quantitative agreement has not been reached yet.[59] A mean deviation of –0.16 V has been found for a series of neutral transition metal complexes, but larger deviations were revealed for highly charged anionic or cationic species. An accurate prediction of the potentials depends also on the simulation of the structure of the reduced and oxidized species as well as on the geometrical conservation during the redox reactions.[60]

The values of E° (which coincides with $E_{1/2}$ when the diffusion coefficients of the oxidized and reduced species are equal), calculated for the half-reactions $[V^{ox}L_2]^{x-} + e^- \rightleftarrows [V^{red}L_2]^{(x+1)-}$, with x = 2 for V^{IV} or x = 1 for V^{V}, were determined with Equation (2):[61]

$$E^\circ = -\left(\frac{\Delta G^\circ_{aq} - \Delta G^\circ_{NHE}}{nF}\right) \quad (2)$$

where ΔG°_{aq} is the Gibbs energy for the specific reduction half-reaction, ΔG°_{NHE} is the Gibbs energy for the reference half-reaction $2H^+ + 2e^- \rightleftarrows H_2$, F is the Faraday constant and n = 1 is the number of exchanged electrons.

DFT results indicate that E° calculated for the couple V^{IV}/V^{III} is –1.50 V, while E° for that V^{V}/V^{IV} is 0.15 V. The value obtained for the reaction $[V^{V}L_2]^{-} + e^- \rightleftarrows [V^{IV}L_2]^{2-}$ is in good agreement with the experimental value of 0.03 V with an absolute deviation of 0.12 V. Concerning the reduction process, $[V^{IV}L_2]^{2-} + e^- \rightleftarrows [V^{III}L_2]^{3-}$, E° is underestimated with a deviation of –0.75 V and this is probably due to the use of a hybrid functional and, above all, to the high negative charge on the species participating to the process.[59]

To investigate the nature of the redox processes, the oxidation state of the metal and to exclude the possible non-innocent behavior of the ligand, further DFT calculations on the orbital localization were carried out using the approach of Boys,[62] recently applied in organometallic chemistry.[63] In Fig-

ure 11 the centroids of the metal localized MOs for the three species involved in the redox processes (V^V, V^{IV}, V^{III}) are shown, while the complete representation of the metal complexes and all the orbital centroids are reported in Figure S9 of the Supporting Information. The determination of the orbital centroids allows to describe where the electrons are and if they belong to the metal or to the ligand.[63]

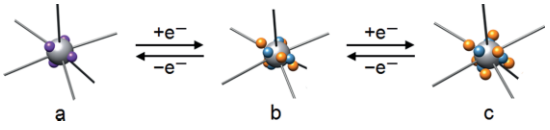

Figure 11. Centroids of the localized orbitals on V for: (a) V^V, (b) V^{IV} and (c) V^{III} species. For V^V (restricted calculation) the electron couples are represented in purple, for V^{IV} and V^{III} (unrestricted calculations) the α and the β electrons are shown in orange and in light blue, respectively.

In $[V^VL_2]^-$ (for which a restricted analysis was performed), there are four centroids localized on V center, representing the occupied semicore 3s and 3p orbitals (a in Figure 11); therefore, the configuration is $3s^23p^6$. Looking at the species derived from one-electron reduction, $[V^{IV}L_2]^{2-}$ (unrestricted analysis, b in Figure 11), it can be observed that five α and four β orbitals (four couples plus an unpaired electrons) are found close to the metal and they can be identified as the semicore fully occupied 3s and 3p orbitals and the singly occupied V-d_{xy} (see also Figure 7); the configuration is $3s^23p^63d^1$. Concerning $[V^{III}L_2]^{3-}$ (unrestricted analysis, c in Figure 11), six α and four β orbitals are localized on V and these can be explained with the configuration $3s^23p^6$ plus two electrons in the V-d orbitals ($3s^23p^63d^2$ configuration for V^{III}). Therefore, on the basis of these results, the oxidation state of V in the three minima can be reasonably described as +V, +IV and +III, with the redox processes essentially metal-based and only assisted by the ligand. The analysis is confirmed by the calculation of the spin density on V atom in the three species: about 0 for V^V, 1.099 for V^{IV} and 1.957 for V^{III}.

Conclusions

In this study the system formed by V^{IV} and glutaroimide–dioxime has been examined in aqueous solution with a number of techniques, instrumental and computational. In particular, a new non-oxido (or bare) V^{IV} complex has been described, enriching the small family of these rare compounds.

The non-oxido species $[V^{IV}L_2]^{2-}$ shows unusual spectroscopic and electrochemical properties, according to the previous results.[15,29] Here we provided to the readers the tools to distinguish a non-oxido V^{IV} complex from a $V^{IV}O$ complex formed by a flexible tridentate ligand such as glutaroimide–dioxime and, also, presented the possible DFT calculations to confirm the results given by the instrumental techniques. Major findings from this study are summarized as follows:

(1) In contrast with $V^{IV}O$, the geometry of bare V^{IV} compounds is not octahedral but intermediate between the octahedron and the trigonal prism. The twist angle Φ (60° for an octahedron and 0° for a trigonal prism) can give information on the entity of the distortion. A DFT calculation at the level of theory B3P86/6-311g gives a good prediction of the structure.

(2) While for an octahedral $V^{IV}O$ complex the energy order of the five V-d orbitals is $d_{xy} < d_{xz} \approx d_{yz} < d_{x^2-y^2} < d_{z^2}$,[52] for these non-oxido V^{IV} species the order is $d_{xy} < d_{xz} \approx d_{yz} < d_{x^2-y^2} \approx d_{z^2}$ with a mixing of V-d_{xy} with the unoccupied V-d orbitals in the SOMO. The shape and composition of the MOs can be calculated by computational methods.

(3) The EPR spectra are characterized by a value of A_i (where A_i is the largest value of the ^{51}V HFC tensor ***A*** and $i = x$ or z, depending on the symmetry of the complex) significantly smaller than that of $V^{IV}O$ species (usually in the range 150–180×10^{-4} cm^{-1}). The experimental value between 120 and 135×10^{-4} cm^{-1} corresponds to a "**type 3**" spectrum, for which a mixing of V-d_{xy}, V-d_{xz} and V-d_{yz} orbitals in the SOMO – which causes a marked lowering of A_i – is expected.[44] The HFC tensor ***A*** can be predicted with a DFT calculation using the functional B2PLYP and the basis sets VTZ or 6-311g(d,p). The value of the angle Ω, formed by the two external donor atoms of the tridentate ligand with vanadium (180° for a *mer* and 90° for a *fac* isomer), could suggest the type of EPR spectrum for this class of compounds.

(4) Differently from $V^{IV}O$ species, for which the bands revealed in the visible region of the electronic absorption spectra are almost pure d–d transitions with very low values of the molar absorption coefficient ε (usually smaller than 200 M^{-1} cm^{-1}), for these bare V^{IV} compounds the d–d bands are expected in the near IR region, whereas in the visible region between 400 and 800 nm the absorptions are mainly metal-to-ligand charge transfer (MLCT) and ligand-to-metal charge transfer (LMCT) transitions (with ε much larger than 1000 M^{-1} cm^{-1}). A DFT simulation at the level of theory CAM-B3LYP/6-31+g(d) allows to obtain a qualitative agreement between the experimental and calculated spectrum and predict the character of the electronic transitions in the UV/Vis spectrum.

(5) For a bare V^{IV} species, two quasi-reversible redox processes can be observed, one toward the reduction to V^{III} in the cathodic region and another toward the oxidation to V^V in the anodic one.[58] These redox processes are assisted by the ligands but are largely metal-based, consistent with previous reports with Mn^{II}/Mn^{III},[64] as well as DFT calculations on the orbital localization, high V-d contribution to the frontier molecular orbitals and spin density on vanadium for the three V^V, V^{IV} and V^{III} complexes. The quasi-reversibility of the processes can be explained considering that the distorted octahedral structure is maintained around V during the redox reactions.[56,57] In contrast, the half-reactions to V^{III} and V^VO_2 would be irreversible for a $V^{IV}O$ complex.[56] The two values of $E_{1/2}$ for the reduction and oxidation measured in a cyclic voltammogram could be predicted in solution (using the SMD, solvation model based on solute electron density) with the B3P86 functional combined with the D3 correction for dispersion, and a general basis set with 6-311g(d,p) for the main group elements and SDD (scalar-relativistic Stuttgart–Dresden pseudopotential) plus *f*-function and pseudopotential for V in the optimization step, and 6-311g++(2d,p) for the main group atoms and quadruple-ζ def2-QZVP for V in the calculation of the Gibbs energy.

Experimental and Computational Section

Chemicals

The glutaroimide–dioxime ligand was synthesized and its purity was verified as described previously.[65] V^{IV} solutions were prepared from $VOSO_4 \cdot 3H_2O$ [oxidovanadium(IV) sulfate trihydrate; 204862], produced by Sigma–Aldrich, following literature methods.[66]

EPR and UV/Vis Measurements

The solutions for EPR and UV/Vis measurements were prepared by dissolving in ultrapure water, obtained through the purification system Millipore MilliQ Academic, a weighted amount of $VOSO_4 \cdot 3H_2O$ and the ligand to obtain a metal ion concentration of 1.0×10^{-3} M and a ligand to metal molar ratio of 3:1. pH was varied with the addition of carbonate-free NaOH solution of known concentration (ca. 0.10 M). Argon was bubbled through the solutions to ensure the absence of oxygen and avoid the oxidation of $V^{IV}O^{2+}$ ion.

EPR spectra were recorded at 120 or 298 K with an X-band (9.4 GHz) Bruker EMX spectrometer equipped with an HP 53150A microwave frequency counter. The microwave frequency used for EPR measurements was in the range of 9.40–9.41 GHz; microwave power was 20 mW, time constant 81.92 ms, modulation frequency 100 kHz, modulation amplitude 0.4 mT, and resolution 4096 points. To extract spin Hamiltonian parameters, the experimental spectra were generated with WinEPR SimFonia software.[43] The values of the ^{51}V hyperfine coupling constants along the *z* axis were compared with those estimated on the basis of the "additivity rule", which relates A_z to the number and type of the equatorial ligands, assigning them a specific contribution. This empirical rule has been proved and accepted in a large number of papers.[34] Usually, the experimental values of A_z fall in the range of $\pm 3 \times 10^{-4}$ cm^{-1} with respect to those estimated with the "additivity rule".[34a,34b] The contributions of RO^- and OH^- donors were taken from refs.[34b,34c], whereas for N^- donor the mean value determined for an amide-N^- was considered.[34c]

The electronic absorption spectra were recorded in the wavelength range 200–800 nm with a Perkin–Elmer Lambda 35 spectrophotometer.

ESI-MS Measurements

ESI-MS measurements were carried out on the system V^{IV}/H_3L at various pH (4–7) with V concentration of 5.0×10^{-6} M. $VOSO_4 \cdot 3H_2O$ was used as precursor of V^{IV} and argon was bubbled inside the aqueous solutions. The solutions containing the metal ion and the ligand were prepared in LC-MS ultrapure water (from Sigma–Aldrich) and the values of pH were eventually varied with $(NH_4)_2CO_3$. ESI-MS and ESI-MS/MS spectra were recorded immediately after the preparation of the solutions.

Mass spectra in the positive and negative ion modes were obtained on a Q Exactive™ Plus Hybrid Quadrupole-Orbitrap™ (Thermo Fisher Scientific) mass spectrometer. The solutions were infused at a flow rate of 5.00 μL min^{-1} into the ESI chamber immediately after their preparation. The spectra were recorded in the *m/z* range 50–750 at a resolution of 140000 and accumulated for at least 5 min to increase the signal-to-noise ratio. The instrumental conditions used for the measurements in positive mode were: spray voltage 2300 V, capillary temperature 250 °C, sheath gas 5–10 (arbitrary units), auxiliary gas 3 (arbitrary units), sweep gas 0 (arbitrary units), probe heater temperature 50 °C. The instrumental conditions for the measurements of the spectra in negative mode were: spray voltage –1900 V, capillary temperature 250 °C, sheath gas 20 (arbitrary units), auxiliary gas 5 (arbitrary units), sweep gas 0 (arbitrary units), probe heater temperature 14 °C.

ESI-MS spectra were analyzed by using Thermo Xcalibur 3.0.63 software (Thermo Fisher Scientific).

Electrochemical Measurements

Cyclic voltammograms on the system V^{IV}/H_3L were recorded with an electrochemical analyzer CH Instruments 600 B at room temperature (25 ± 1 °C) in H_2O with 0.1 M KNO_3 at the same experimental conditions (pH and ligand to metal molar ratio) used to record EPR and electronic absorption spectra. The total V^{IV} concentration was 1.0×10^{-3} M. A Pt working electrode, a Pt wire counter electrode and an Ag/AgCl reference were employed. All potentials were calculated relative to the Ag/AgCl electrode (0.20 V vs. normal hydrogen electrode, NHE), with a value of +0.26 V for the $[Fe(CN)_6]^{3-/4-}$ couple (0.01 M NaOH). Voltammograms were obtained at scan rates between 0.01 and 1 V s^{-1}. Redox potentials were determined with a precision of ± 0.01 V. The experimental conditions for the electrochemistry measurements of the reported systems were detailed in the refs.[22a,50,51,57] even if comparisons are subject to the variations in the experimental conditions.[67]

DFT Calculations

The calculations presented in this study were performed with DFT methods using the software Gaussian 09 (rev. C.01)[68] and ORCA (vers. 4.0).[69]

The pK_a values were computed with Gaussian 09 using the hybrid B3LYP functional[70] combined with the Grimme's D3 correction[71] for dispersion and the 6-311++g(d,p) basis set. The solvent effect was taken into account for the single point calculations adopting the SMD continuum model of Marenich et al.[72] An explicit cluster of water molecules was adopted to take into account the solvent stabilization of the acid groups, and their number was constant during all cycles (9 water molecules solvating the oxime groups N–OH and 2 the imide NH_2^+).

The geometry of $[V^{IV}L_2]^{2-}$, $[V^{V}L_2]^{-}$ and $[V^{IV}OL(OH)]^{2-}$ complexes was optimized with Gaussian 09 with the functional B3P86[70a,73] and the basis set 6-311g or 6-311++g(d,p) with the procedure reported in the literature.[42,74] This choice ensures a good degree of accuracy in the prediction of the structures of first-row transition metal complexes[75] and, in particular, of vanadium compounds.[42] For all the structures, minima were verified through frequency calculations. Cartesian coordinates obtained from the geometry optimization are available in Tables S2–S6 of the Supporting Information.

On the optimized structures, the ^{51}V hyperfine coupling tensor $\boldsymbol{A}$ was calculated with ORCA software. For $V^{IV}O$ complexes the functional PBE0[76] and the basis set VTZ were used, while for bare V^{IV} species the double hybrid functional B2PLYP (that includes a second-order perturbation correction for nonlocal correlation effects)[47] coupled with the basis set VTZ (for A_{iso}) or 6-311g(d,p) (for A_x, A_y and A_z) were employed. It must be taken into account that for a V^{IV} species the value of *A* is usually negative, but in the literature its absolute value is often reported; this formalism was also used in a number of points of this study. The ^{51}V HFC tensor $\boldsymbol{A}$ has three contributions: the isotropic Fermi contact (A^{FC}), the anisotropic or dipolar hyperfine interaction ($\boldsymbol{A}^{D}$) and the second-order term that arises from spin–orbit (SO) coupling ($\boldsymbol{A}^{SO}$):[69b] $\boldsymbol{A} = A^{FC}\boldsymbol{1} + \boldsymbol{A}^{D} + \boldsymbol{A}^{SO}$, where $\boldsymbol{1}$ is the unit tensor. The values of the ^{51}V anisotropic hyperfine coupling constants along the *x*, *y*, and *z* axes are $A_x = A^{FC} + A_x^{D} + A_x^{SO}$, $A_y = A^{FC} + A_y^{D} + A_y^{SO}$ and $A_z = A^{FC} + A_z^{D} + A_z^{SO}$. From these equations, the value of A_{iso} is $A_{iso} = (1/3)(A_x + A_y + A_z) = A^{FC} + (1/3)(A_x^{SO} + A_y^{SO} + A_z^{SO})$.[69b] The theory background was described in detail in refs.[35,44,77]. The percent deviation (PD) of the absolute calculated value, $|A_i|^{calcd}$, from the absolute experimental

value, $|A_i|^{exptl}$, was obtained as follows: $100 \times [(|A_i|^{calcd} - |A_i|^{exptl})/|A_i|^{exptl}]$, with i = iso or z.

Time-dependent density functional theory (TD-DFT) calculations[78] were used to predict the excited states of $[V^{IV}L_2]^{2-}$ and obtain the expected electronic absorption spectrum. The calculations were carried out on the geometry optimized in the gas phase using CAM-B3LYP functional and 6-31+g(d) basis set, according to the method established previously.[27]

The structures of V^V, V^{IV} and V^{III} species used to calculate E^o [see formula (2)] were optimized in aqueous solution with SMD continuum model[72] using the B3P86 functional combined with the Grimme's D3 correction for dispersion,[71] and the basis set 6-311g(d,p) for the main group elements and SDD plus *f*-function[79] and pseudopotential for vanadium. Cartesian coordinates of the optimized structures for V^V, V^{IV} and V^{III} are reported in Tables S7–S9 of the Supporting Information. The Gibbs energy in solution (ΔG^o_{aq}) of the species was estimated through single point calculations expanding the basis set for the main group atoms to 6-311g++(2d,p) and for V to the quadruple-ζ def2-QZVP. For the half-cell proton reduction, ΔG^o_{NHE}, the value of –412.96 kJ mol^{-1} was used.[61] The values of E^o, calculated in the text for the reactions $[V^VL_2]^- + e^- \rightleftarrows [V^{IV}L_2]^{2-}$ and $[V^{IV}L_2]^{2-} + e^- \rightleftarrows [V^{III}L_2]^{3-}$, were corrected with the potential of the Ag/AgCl electrode (0.20 V vs. NHE).

Orbital localization was performed by DFT methods through the CP2K software,[80] using the PBE exchange-correlation functional.[76a] Only the valence electrons were included in the simulations, employing the GTH-type pseudopotentials;[81] in particular, for V the semicore $3s^23p^6$ and the valence $3d^34s^2$ electrons were considered explicitly. For V^V complex, $[V^VL_2]^-$ with $S = 0$, a restricted calculation was performed, while V^{IV} and V^{III} species, $[V^{IV}L_2]^{2-}$ with $S = 1/2$ and $[V^{III}L_2]^{3-}$ with $S = 1$, were treated with an unrestricted analysis.

Conflicts of Interest

There are no conflicts to declare.

Acknowledgments

D. S., V. U., and E. G. thank Fondazione di Sardegna (FdS15Garribba) for the financial support, and G. S. thanks Universitat Autònoma de Barcelona for supporting his Ph.D. grant. B. F. P., Z. Z., C. J. L., J. A., and L. R. were supported by the Fuel Cycle Research and Development Campaign (FCRD)/Fuel Resources Program, Office of Nuclear Energy, the U.S. Department of Energy (USDOE) under Contract No. DE-AC02-05CH11231 at Lawrence Berkeley National Laboratory (LBNL).

Keywords: Vanadium · Oxides · EPR spectroscopy · Density functional calculations · Redox chemistry

[1] F. H. Nielsen in *Vanadium Compounds: Chemistry, Biochemistry and Therapeutic Applications, Vol. 711* (Eds.), American Chemical Society, **1998**, pp. 297–307.
[2] J. Costa Pessoa, I. Tomaz, *Curr. Med. Chem.* **2010**, *17*, 3701–3738.
[3] D. Rehder, *Future Med. Chem.* **2012**, *4*, 1823–1837.
[4] J. Costa Pessoa, S. Etcheverry, D. Gambino, *Coord. Chem. Rev.* **2015**, *301–302*, 24–48.
[5] Y. Yoshikawa, H. Sakurai, D. C. Crans, G. Micera, E. Garribba, *Dalton Trans.* **2014**, *43*, 6965–6972.
[6] a) A. Levina, D. C. Crans, P. A. Lay, *Coord. Chem. Rev.* **2017**, *352*, 473–498; b) A. Levina, A. I. McLeod, S. J. Gasparini, A. Nguyen, W. G. M. De Silva, J. B. Aitken, H. H. Harris, C. Glover, B. Johannessen, P. A. Lay, *Inorg. Chem.* **2015**, *54*, 7753–7766.
[7] D. Rehder, *Future Med. Chem.* **2016**, *8*, 325–338.
[8] a) K. H. Thompson, C. Orvig, *Coord. Chem. Rev.* **2001**, *219–221*, 1033–1053; b) Y. Shechter, I. Goldwaser, M. Mironchik, M. Fridkin, D. Gefel, *Coord. Chem. Rev.* **2003**, *237*, 3–11; c) K. H. Thompson, C. Orvig, *J. Inorg. Biochem.* **2006**, *100*, 1925–1935.
[9] a) D. Sanna, G. Micera, E. Garribba, *Inorg. Chem.* **2013**, *52*, 11975–11985; b) D. Sanna, G. Micera, E. Garribba, *Inorg. Chem.* **2014**, *53*, 1449–1464; c) M. F. A. Santos, I. Correia, A. R. Oliveira, E. Garribba, J. Costa Pessoa, T. Santos-Silva, *Eur. J. Inorg. Chem.* **2014**, 3293–3297; d) J. Costa Pessoa, E. Garribba, M. F. A. Santos, T. Santos-Silva, *Coord. Chem. Rev.* **2015**, *301–302*, 49–86.
[10] D. C. Crans, J. J. Smee, E. Gaidamauskas, L. Yang, *Chem. Rev.* **2004**, *104*, 849–902.
[11] a) H. Vilter in *Met. Ions Biol. Syst., Vol. 31* (Eds.: H. Sigel, A. Sigel), Marcel Dekker, New York, **1995**, pp. 325–362; b) V. L. Pecoraro, C. Slebodnick, B. Hamstra in *Vanadium Compounds: Chemistry, Biochemistry and Therapeutic Applications*, *Vol. 711*, American Chemical Society, **1998**, pp. 157–167.
[12] a) R. L. Robson, R. R. Eady, T. H. Richardson, R. W. Miller, M. Hawkins, J. R. Postgate, *Nature* **1986**, *322*, 388–390; b) R. R. Eady, *Coord. Chem. Rev.* **2003**, *237*, 23–30.
[13] a) T. Ueki, H. Michibata, *Coord. Chem. Rev.* **2011**, *255*, 2249–2257; b) D. Fattorini, F. Regoli in *Vanadium. Biochemical and Molecular Biological Approaches* (Ed.: H. Michibata), Springer Netherlands, **2012**, pp. 73–92.
[14] J. A. L. da Silva, J. J. R. Fraústo da Silva, A. J. L. Pombeiro in *Vanadium. Biochemical and Molecular Biological Approaches* (Ed.: H. Michibata), Springer Netherlands, **2012**, pp. 35–49.
[15] D. Rehder, *Bioinorganic Vanadium Chemistry*, John Wiley & Sons, Ltd, Chichester, **2008**.
[16] H. Kneifel, E. Bayer, *Angew. Chem. Int. Ed. Engl.* **1973**, *12*, 508–508; *Angew. Chem.* **1973**, *85*, 542–543.
[17] J. A. L. da Silva, J. J. R. Fraústo da Silva, A. J. L. Pombeiro, *Coord. Chem. Rev.* **2013**, *257*, 2388–2400.
[18] P. M. Reis, J. A. L. da Silva, J. J. R. Fraústo da Silva, A. J. L. Pombeiro, *Chem. Commun.* **2000**, 1845–1846.
[19] P. M. Reis, J. A. L. da Silva, J. J. R. Fraústo da Silva, A. J. L. Pombeiro, *J. Mol. Catal. A* **2004**, *224*, 189–195.
[20] a) M. V. Kirillova, M. L. Kuznetsov, P. M. Reis, J. A. L. da Silva, J. J. R. Fraústo da Silva, A. J. L. Pombeiro, *J. Am. Chem. Soc.* **2007**, *129*, 10531–10545; b) P. M. Reis, J. A. L. da Silva, A. F. Palavra, J. J. R. Fraústo da Silva, T. Kitamura, Y. Fujiwara, A. J. L. Pombeiro, *Angew. Chem. Int. Ed.* **2003**, *42*, 821–823; *Angew. Chem.* **2003**, *115*, 845–847.
[21] P. R. Klich, A. T. Daniher, P. R. Challen, D. B. McConville, W. J. Youngs, *Inorg. Chem.* **1996**, *35*, 347–356.
[22] a) S. R. Cooper, Y. B. Koh, K. N. Raymond, *J. Am. Chem. Soc.* **1982**, *104*, 5092–5102; b) T. B. Karpishin, T. D. P. Stack, K. N. Raymond, *J. Am. Chem. Soc.* **1993**, *115*, 182–192.
[23] a) E. I. Stiefel, Z. Dori, H. B. Gray, *J. Am. Chem. Soc.* **1967**, *89*, 3353–3354; b) W. E. Broderick, E. M. McGhee, M. R. Godfrey, B. M. Hoffman, J. A. Ibers, *Inorg. Chem.* **1989**, *28*, 2902–2904; c) M. Kondo, S. Minakoshi, K. Iwata, T. Shimizu, H. Matsuzaka, N. Kamigata, S. Kitagawa, *Chem. Lett.* **1996**, *25*, 489–490.
[24] a) A. A. Diamantis, M. R. Snow, J. A. Vanzo, *J. Chem. Soc., Chem. Commun.* **1976**, 264–265; b) E. Ludwig, H. Hefele, E. Uhlemann, F. Weller, W. Kläi, *Z. Anorg. Allg. Chem.* **1995**, *621*, 23–28; c) T. K. Paine, T. Weyhermüller, E. Bill, E. Bothe, P. Chaudhuri, *Eur. J. Inorg. Chem.* **2003**, 4299–4307.
[25] T. K. Paine, T. Weyhermüller, L. D. Slep, F. Neese, E. Bill, E. Bothe, K. Wieghardt, P. Chaudhuri, *Inorg. Chem.* **2004**, *43*, 7324–7338.
[26] J. G. Reynolds, E. L. Jones, J. C. Huffman, G. Christou, *Polyhedron* **1993**, *12*, 407–414.
[27] S. Kundu, D. Mondal, K. Bhattacharya, A. Endo, D. Sanna, E. Garribba, M. Chaudhury, *Inorg. Chem.* **2015**, *54*, 6203–6215.
[28] A. Diamantis, M. Manikas, M. Salam, M. Snow, E. Tiekink, *Aust. J. Chem.* **1988**, *41*, 453–468.
[29] G. Micera, D. Sanna in *Vanadium in the Environment Part I: Chemistry and Biochemistry* (Ed.: J. O. Nriagu), Wiley, New York, **1998**, pp. 131–166.
[30] C. J. Leggett, B. F. Parker, S. J. Teat, Z. Zhang, P. D. Dau, W. W. Lukens, S. M. Peterson, A. J. P. Cardenas, M. G. Warner, J. K. Gibson, J. Arnold, L. Rao, *Chem. Sci.* **2016**, *7*, 2775–2786.

[31] a) G. Tian, S. J. Teat, Z. Zhang, L. Rao, *Dalton Trans.* **2012**, *41*, 11579–11586; b) S. A. Ansari, Y. Yang, Z. Zhang, K. J. Gagnon, S. J. Teat, S. Luo, L. Rao, *Inorg. Chem.* **2016**, *55*, 1315–1323.
[32] M. D. Liptak, G. C. Shields, *J. Am. Chem. Soc.* **2001**, *123*, 7314–7319.
[33] a) R. P. Henry, P. C. H. Mitchell, J. E. Prue, *J. Chem. Soc., Dalton Trans.* **1973**, 1156–1159; b) A. Komura, M. Hayashi, H. Imanaga, *Bull. Chem. Soc. Jpn.* **1977**, *50*, 2927–2931; c) L. F. C. P. Vilas Boas in *Comprehensive Coordination Chemistry, Vol. 3* (Eds.: G. Wilkinson, R. D. Gillard, J. A. McCleverty), Pergamon Press, Oxford, **1985**, pp. 453–583.
[34] a) D. N. Chasteen in *Biological Magnetic Resonance, Vol. 3* (Eds.: L. J. J. Berliner, J. Reuben), Plenum Press, New York, **1981**, pp. 53–119; b) T. S. Smith II, R. LoBrutto, V. L. Pecoraro, *Coord. Chem. Rev.* **2002**, *228*, 1–18; c) E. Garribba, E. Lodyga-Chruscinska, G. Micera, A. Panzanelli, D. Sanna, *Eur. J. Inorg. Chem.* **2005**, 1369–1382.
[35] G. Micera, E. Garribba, *J. Comput. Chem.* **2011**, *32*, 2822–2835.
[36] L. E. Sojo, N. Chahal, B. O. Keller, *Rapid Commun. Mass Spectrom.* **2014**, *28*, 2181–2190.
[37] a) D. Sanna, V. Ugone, G. Micera, P. Buglyo, L. Biro, E. Garribba, *Dalton Trans.* **2017**, *46*, 8950–8967; b) D. Sanna, V. Ugone, G. Sciortino, P. Buglyo, Z. Bihari, P. L. Parajdi-Losonczi, E. Garribba, *Dalton Trans.* **2018**, *47*, 2164–2182.
[38] L. Pisano, K. Varnagy, S. Timári, K. Hegetschweiler, G. Micera, E. Garribba, *Inorg. Chem.* **2013**, *52*, 5260–5272.
[39] S. Steinhauser, U. Heinz, M. Bartholomä, T. Weyhermüller, H. Nick, K. Hegetschweiler, *Eur. J. Inorg. Chem.* **2004**, 4177–4192.
[40] S. Steinhauser, U. Heinz, J. Sander, K. Hegetschweiler, *Z. Anorg. Allg. Chem.* **2004**, *630*, 1829–1838.
[41] A. Castiñeiras Campos, A. G. Silica Zafra, J. M. González Pérez, J. Niclós Gutiérrez, E. Chinea, A. Mederos, *Inorg. Chim. Acta* **1996**, *241*, 39–45.
[42] G. Micera, E. Garribba, *Int. J. Quantum Chem.* **2012**, *112*, 2486–2498.
[43] *WINEPR SimFonia, version 1.25*, Bruker Analytische Messtechnik GmbH, Karlsruhe, **1996**.
[44] D. Sanna, G. Sciortino, V. Ugone, G. Micera, E. Garribba, *Inorg. Chem.* **2016**, *55*, 7373–7387.
[45] D. Sanna, K. Várnagy, N. Lihi, G. Micera, E. Garribba, *Inorg. Chem.* **2013**, *52*, 8202–8213.
[46] E. Lodyga-Chruscinska, A. Szebesczyk, D. Sanna, K. Hegetschweiler, G. Micera, E. Garribba, *Dalton Trans.* **2013**, *42*, 13404–13416.
[47] S. Grimme, *J. Chem. Phys.* **2006**, *124*, 034108.
[48] G. Micera, E. Garribba, *Dalton Trans.* **2009**, 1914–1918.
[49] S. P. Dash, S. Majumder, A. Banerjee, M. F. N. N. Carvalho, P. Adão, J. Costa Pessoa, K. Brzezinski, E. Garribba, H. Reuter, R. Dinda, *Inorg. Chem.* **2016**, *55*, 1165–1182.
[50] B. Morgenstern, S. Steinhauser, K. Hegetschweiler, E. Garribba, G. Micera, D. Sanna, L. Nagy, *Inorg. Chem.* **2004**, *43*, 3116–3126.
[51] B. Morgenstern, B. Kutzky, C. Neis, S. Stucky, K. Hegetschweiler, E. Garribba, G. Micera, *Inorg. Chem.* **2007**, *46*, 3903–3915.
[52] C. J. Ballhausen, H. B. Gray, *Inorg. Chem.* **1962**, *1*, 111–122.
[53] A. Desideri, J. B. Raynor, A. A. Diamantis, *J. Chem. Soc., Dalton Trans.* **1978**, 423–426.
[54] a) E. Lodyga-Chruscinska, D. Sanna, E. Garribba, G. Micera, *Dalton Trans.* **2008**, 4903–4916; b) G. Micera, E. Garribba, *Eur. J. Inorg. Chem.* **2010**, 4697–4710; c) G. Micera, E. Garribba, *Eur. J. Inorg. Chem.* **2011**, 3768–3780; d) D. Sanna, K. Varnágy, S. Timári, G. Micera, E. Garribba, *Inorg. Chem.* **2011**, *50*, 10328–10341; e) D. Sanna, V. Ugone, G. Micera, E. Garribba, *Dalton Trans.* **2012**, *41*, 7304–7318.
[55] T. B. Karpishin, T. M. Dewey, K. N. Raymond, *J. Am. Chem. Soc.* **1993**, *115*, 1842–1851.
[56] a) J. Selbin, *Chem. Rev.* **1965**, *65*, 153–175; b) J. Selbin, *Coord. Chem. Rev.* **1966**, *1*, 293–314.
[57] A. Friedrich, H. Hefele, W. Mickler, A. Mönner, E. Uhlemann, F. Scholz, *Electroanalysis* **1998**, *10*, 244–248.
[58] P. Galloni, V. Conte, B. Floris, *Coord. Chem. Rev.* **2015**, *301–302*, 240–299.
[59] L. E. Roy, E. Jakubikova, M. G. Guthrie, E. R. Batista, *J. Phys. Chem. A* **2009**, *113*, 6745–6750.
[60] L. Yan, Y. Lu, X. Li, *Phys. Chem. Chem. Phys.* **2016**, *18*, 5529–5536.
[61] P. Jaque, A. V. Marenich, C. J. Cramer, D. G. Truhlar, *J. Phys. Chem. C* **2007**, *111*, 5783–5799.
[62] a) S. F. Boys, *Rev. Mod. Phys.* **1960**, *32*, 296–299; b) J. M. Foster, S. F. Boys, *Rev. Mod. Phys.* **1960**, *32*, 300–302.
[63] P. Vidossich, A. Lledós, *Dalton Trans.* **2014**, *43*, 11145–11151.
[64] X. Xie, Y. Tian, Z. Qin, Q. Yu, H. Wei, D. Wang, X. Li, X. Wang, *Sci. Rep.* **2017**, *7*, 43503.
[65] C. J. Leggett, L. Rao, *Polyhedron* **2015**, *95*, 54–59.
[66] I. Nagypál, I. Fábián, *Inorg. Chim. Acta* **1982**, *61*, 109–113.
[67] I. Noviandri, R. D. Bolskar, P. A. Lay, C. A. Reed, *J. Phys. Chem. B* **1997**, *101*, 6350–6358.
[68] M. J. Frisch, G. W. Trucks, H. B. Schlegel, G. E. Scuseria, M. A. Robb, J. R. Cheeseman, G. Scalmani, V. Barone, B. Mennucci, G. A. Petersson, H. Nakatsuji, M. Caricato, X. Li, H. P. Hratchian, A. F. Izmaylov, J. Bloino, G. Zheng, J. L. Sonnenberg, M. Hada, M. Ehara, K. Toyota, R. Fukuda, J. Hasegawa, M. Ishida, T. Nakajima, Y. Honda, O. Kitao, H. Nakai, T. Vreven, J. A. Montgomery Jr., J. E. Peralta, F. Ogliaro, M. Bearpark, J. J. Heyd, E. Brothers, K. N. Kudin, V. N. Staroverov, R. Kobayashi, J. Normand, K. Raghavachari, A. Rendell, J. C. Burant, S. S. Iyengar, J. Tomasi, M. Cossi, N. Rega, J. M. Millam, M. Klene, J. E. Knox, J. B. Cross, V. Bakken, C. Adamo, J. Jaramillo, R. Gomperts, R. E. Stratmann, O. Yazyev, A. J. Austin, R. Cammi, C. Pomelli, J. W. Ochterski, R. L. Martin, K. Morokuma, V. G. Zakrzewski, G. A. Voth, P. Salvador, J. J. Dannenberg, S. Dapprich, A. D. Daniels, Ö. Farkas, J. B. Foresman, J. V. Ortiz, J. Cioslowski, D. J. Fox, *Gaussian 09, Revision C.01*, Gaussian, Inc., Wallingford CT, **2010**.
[69] a) F. Neese, *Wiley Interdiscip. Rev. Comput. Mol. Sci.* **2012**, *2*, 73–78; b) F. Neese, *ORCA - An Ab Initio, DFT and Semiempirical Program Package, Version 4.0*, Max-Planck-Institute for Chemical Energy Conversion, Mülheim a. d. Ruhr, **2017**.
[70] a) A. D. Becke, *J. Chem. Phys.* **1993**, *98*, 5648–5652; b) C. Lee, W. Yang, R. G. Parr, *Phys. Rev. B* **1988**, *37*, 785–789.
[71] S. Grimme, J. Antony, S. Ehrlich, H. Krieg, *J. Chem. Phys.* **2010**, *132*, 154104.
[72] A. V. Marenich, C. J. Cramer, D. G. Truhlar, *J. Phys. Chem. B* **2009**, *113*, 6378–6396.
[73] a) J. P. Perdew, *Phys. Rev. B* **1986**, *33*, 8822–8824; b) J. P. Perdew, *Phys. Rev. B* **1986**, *34*, 7406–7406.
[74] a) D. Sanna, P. Buglyó, L. Bíró, G. Micera, E. Garribba, *Eur. J. Inorg. Chem.* **2012**, 1079–1092; b) D. Sanna, L. Biro, P. Buglyo, G. Micera, E. Garribba, *Metallomics* **2012**, *4*, 33–36; c) D. Sanna, L. Bíró, P. Buglyó, G. Micera, E. Garribba, *J. Inorg. Biochem.* **2012**, *115*, 87–99; d) D. Sanna, V. Pecoraro, G. Micera, E. Garribba, *J. Biol. Inorg. Chem.* **2012**, *17*, 773–790; e) D. Sanna, P. Buglyo, A. I. Tomaz, J. Costa Pessoa, S. Borovic, G. Micera, E. Garribba, *Dalton Trans.* **2012**, *41*, 12824–12838.
[75] a) M. Bühl, H. Kabrede, *J. Chem. Theory Comput.* **2006**, *2*, 1282–1290; b) M. Bühl, C. Reimann, D. A. Pantazis, T. Bredow, F. Neese, *J. Chem. Theory Comput.* **2008**, *4*, 1449–1459.
[76] a) J. P. Perdew, K. Burke, M. Ernzerhof, *Phys. Rev. Lett.* **1996**, *77*, 3865–3868; b) J. P. Perdew, K. Burke, M. Ernzerhof, *Phys. Rev. Lett.* **1997**, *78*, 1396–1396.
[77] S. Gorelsky, G. Micera, E. Garribba, *Chem. Eur. J.* **2010**, *16*, 8167–8180.
[78] E. Runge, E. K. U. Gross, *Phys. Rev. Lett.* **1984**, *52*, 997–1000.
[79] A. W. Ehlers, M. Böhme, S. Dapprich, A. Gobbi, A. Höllwarth, V. Jonas, K. F. Köhler, R. Stegmann, A. Veldkamp, G. Frenking, *Chem. Phys. Lett.* **1993**, *208*, 111–114.
[80] J. VandeVondele, M. Krack, F. Mohamed, M. Parrinello, T. Chassaing, J. Hutter, *Comput. Phys. Commun.* **2005**, *167*, 103–128.
[81] a) S. Goedecker, M. Teter, J. Hutter, *Phys. Rev. B* **1996**, *54*, 1703–1710; b) C. Hartwigsen, S. Goedecker, J. Hutter, *Phys. Rev. B* **1998**, *58*, 3641–3662; c) M. Krack, *Theor. Chem. Acc.* **2005**, *114*, 145–152.

Received: January 21, 2018

